Downgoing plate topography stopped rupture in the A.D. 2005 Sumatra earthquake

Timothy J. Henstock[1], Lisa C. McNeill[1], Jonathan M. Bull[1], Becky J. Cook[1], Sean P.S. Gulick[2], James A. Austin, Jr.[2], Haryadi Permana[3], and Yusuf S. Djajadihardja[4]

[1]National Oceanography Centre Southampton, University of Southampton, European Way, Southampton SO14 3ZH, UK
[2]Institute for Geophysics, Jackson School of Geosciences, University of Texas at Austin, J.J. Pickle Research Campus Building 196, 10100 Burnett Road, Austin, Texas 78758-4445, USA
[3]Research Center for Geotechnology, Indonesia Institute of Sciences, LIPI Complex, Jl. Cisitu Sangkuriang, Bandung 40135, Indonesia
[4]Geospatial Data Agency, Bakosurtanal, Jl. Raya Jakarta, Bogor KM 46, Cibinong 16911, Indonesia

ABSTRACT

Earthquakes in subduction zones rupture the plate boundary fault in discrete segments. One factor that may control this segmentation is topography on the downgoing plate, although it is controversial whether this is by weakening or strengthening of the fault. We use multichannel seismic and gravity data to map the top of the downgoing oceanic crust offshore central Sumatra, Indonesia. Our survey spans a complex segment boundary zone between the southern termination of the M_w = 8.7, A.D. 2005 Simeulue-Nias earthquake, and the northern termination of a major 1797 earthquake that was partly filled by an M_w = 7.7 event in 1935. We identify an isolated 3 km basement high at the northern edge of this zone, close to the 2005 slip termination. The high probably originated at the Wharton fossil ridge, and is almost aseismic in both local and global data sets, suggesting that while the region around it may be weakened by fracturing and fluids, the basement high locally strengthens the plate boundary, stopping rupture propagation.

INTRODUCTION

Subduction zones are known to rupture in distinct sections or segments. Links between topography on the downgoing plate and this segmentation are debated (Wang and Bilek, 2011; Kopp, 2013). Topography exceeding 1 km correlates with segment boundaries west of South America (Sparkes et al., 2010), but the mechanism, whether by changing mechanical coupling or fault zone physical properties, remains controversial. Some studies argue that subducting topography exceeding the height of the décollement zone strengthens the plate boundary, increasing coupling and acting as a seismic asperity (Cloos, 1992; Scholz and Small, 1997; Bilek et al., 2003); others argue that subducting topography fractures and increases fluid content in the overriding plate, decreasing coupling and limiting strain accumulation to suppress seismogenic rupture (Kelleher and McCann, 1976; Wang and Bilek, 2011; Singh et al., 2011). More detailed observations suggest that some subducted seamounts concentrate stress ahead of them but suppress seismicity above and behind due to fracturing (Mochizuki et al., 2008) and that accompanying erosion of the overriding plate results from hydrofracture (von Huene et al., 2004).

A key issue is that there are few examples where rupture during a major earthquake and topography of the plate boundary within the seismogenic zone are both well constrained. Here we examine a dense network of seismic reflection and gravity data from the central Sunda subduction zone to constrain the depth to the top of the downgoing plate. This region spans the termination of the 28 March 2005, M_w 8.7 earthquake with well-characterized slip distribution. We show that the southern end of the 2005 rupture corresponds to a 3 km high on the downgoing plate originating at the Wharton fossil ridge.

TECTONIC SETTING OF THE SUMATRA MARGIN

The central Sumatra margin had major earthquakes in 1797, 1833, and 1861 (Newcomb and McCann, 1987) as well as the modern events since 2004 (Fig. 1). Coral uplift constrains the extent of the M_w = 8.7–8.9

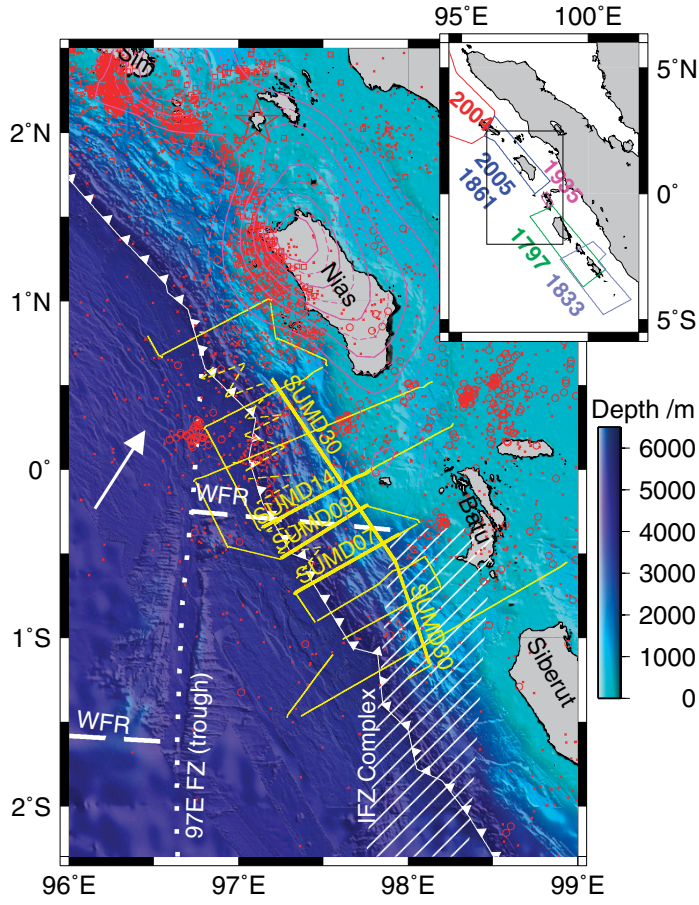

Figure 1. Swath bathymetry superimposed on global topography with magenta contours of A.D. 2005 Sumatra (Indonesia) earthquake coseismic slip from Hsu et al. (2006). Dashed lines are at 1 m intervals and solid lines are at 2 m intervals; red star is epicenter. Red symbols show earthquake epicenters, circles (Lange et al., 2010) and squares (Tilmann et al., 2010) show local studies, and small x symbols indicate the International Seismological Centre catalogue 1960–2013 (http://www.isc.ac.uk/). The 97E fracture zone (97E FZ) and Investigator fracture zone (IFZ) (Kopp et al., 2008) are yellow dotted lines and hachures, respectively. Yellow dashed lines are segments of the Wharton fossil ridge (WFR) modified after Liu et al. (1983), based on our bathymetry. Yellow lines show multichannel seismic reflection profiles (solid line is cruise SO198–2, dashed line is cruise SO200, heavy lines are the profiles in Fig. 2). The downgoing plate moves in the direction of the arrow at 40–45 mm/yr relative to the forearc sliver (McNeill and Henstock, 2014). Inset is regional tectonic setting, showing slip areas for the A.D. 1797, 1833, 1935 (Natawidjaja et al., 2006), 2004, and 2005 earthquakes.

Data Repository item 2016017 | doi:10.1130/G37258.

1797 earthquake centered on Siberut Island and the M_w = 8.9–9.1 1833 earthquake further to the south, but with overlapping rupture areas (Natawidjaja et al., 2006). A smaller M_w = 7.7 earthquake in 1935 ruptured an area near the Batu Islands, a section unaffected by either the 1797 or 1861 events (Natawidjaja et al., 2004). Geodetic and seismic data sets give good constraints on slip during the 2005 earthquake, which ruptured the plate boundary from central Simeulue Island to just south of Nias Island (repeating the 1861 rupture area; Meltzner et al., 2015), with maximum slip of 10 m (Hsu et al., 2006; Fig. 1).

The subducting oceanic crust on this part of the margin formed at the Wharton fossil ridge (WFR, Fig. 1) at 50–35 Ma (Jacob et al., 2014). Spreading rates at 50 Ma were as high as 120 mm/yr full rate (Jacob et al., 2014), and decreased after 45 Ma due to plate reorganization, which led to abandonment of the WFR (Liu et al., 1983); the final spreading rate was as slow as 40 mm/yr (Jacob et al., 2014). At these slow spreading rates, ridge-parallel normal faulting is expected, with fracture zones having thin crust and deep topography. North-south fracture zones can be identified in both the free air gravity field (Royer and Sandwell, 1989) and in swath bathymetry outboard of the trench (Kopp et al., 2008; Fig. 1). Complex topography of the Investigator fracture zone (IFZ) intersects the margin offshore Siberut; the 97E fracture zone (97EFZ; trough in Fig. 1) intersects the margin offshore Nias, with a section of the relict WFR intersecting the margin offshore the Batu Islands (Liu et al., 1983; Fig. 1). Convergence between the downgoing plate and the forearc sliver is 40–45 mm/yr at 25° north of perpendicular (McNeill and Henstock, 2014; Fig. 1). The intersections of fracture zones with the margin move southward with time while sections of the WFR move northward.

Chlieh et al. (2008) inferred heterogeneous geodetic coupling on the plate boundary (from 100% beneath Nias and Siberut to 40% beneath the Batu Islands) and suggested that low coupling causes continuous strain release and a persistent segment boundary zone, perhaps due to topography of the subducted IFZ (Chlieh et al., 2008). Nevertheless, 2–3 m of coseismic slip occurred beneath the Batu Islands in 1935 and the pattern of interseismic slip is temporally and spatially complex (Natawidjaja et al., 2006). Longer term measurements suggest that the plate boundary coupling is high throughout the region (Prawirodirdjo et al., 2010).

BASEMENT TOPOGRAPHY FROM SEISMIC REFLECTION DATA

We have imaged the top of the downgoing plate using multichannel seismic reflection (MCS) profiles collected during R/V *Sonne* cruises SO198–2 and SO200. During expedition SO198–2, we used a 5420 in^3 airgun source at a pressure of 2100 psi fired at intervals of 20 s (~50 m shotpoint spacing), recorded on a 2.4 km, 192 channel hydrophone streamer. During SO200, we used a 1400 in^3 airgun source at a pressure of 2100 psi, fired at intervals of 10–15 s, and a 300 m, 24 channel hydrophone streamer. For both data sets, we used simple data processing: geometry assignment at 6.25 m common midpoint interval, swell noise suppression, bandpass filter, predictive deconvolution, true amplitude recovery, normal moveout correction, and stacking. After stacking, we enhanced features at depth with an additional bandpass filter, frequency-wavenumber filter to suppress scattered energy, and automatic gain control with a 2.5 s window. We converted to depth using a seismic velocity of 1.5 km/s above the seabed, increasing linearly from 2 to 5 km/s from the seabed to 5 km beneath the seabed, then fixed at 5 km/s. These velocities are consistent with seismic refraction results between Simeulue and Nias (Kieckhefer et al., 1980; Shulgin et al., 2013) and remove most effects of seabed bathymetry without introducing artifacts in the deeper structure. This approach is more robust to assumptions about seismic velocity than prestack depth migration; however, it limits lateral resolution to the Fresnel zone of ~4 km.

Immediately west of the trench, spreading ridge normal faults are imaged in the bathymetry on either side of the 97EFZ (Fig. 1). Sediment thickens eastward to 2.5–3 km at the deformation front (Fig. 2). The MCS profiles (Fig. 2; Figs. DR1 and DR2 in the GSA Data Re-

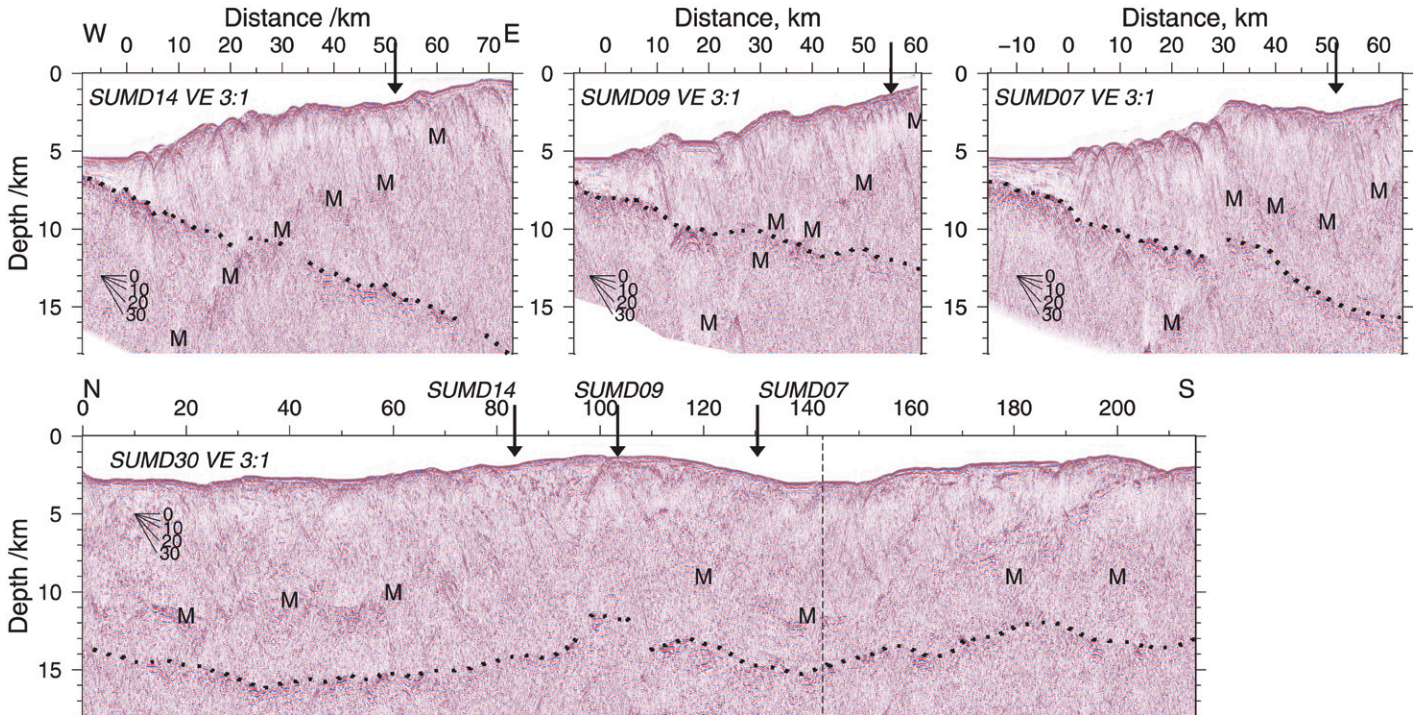

Figure 2. Depth-converted seismic reflection sections. The deformation front is at 0 km on each of the three dip profiles (SUMD07, SUMD09, SUMD14); the black arrow shows the intersection of strike profile SUMD30. VE—vertical exaggeration. Dotted lines show the top of the oceanic basement; M is the seabed multiple.

pository[1]) show that the prism consists of a series of thrust-controlled folds with minimal surficial sediment. The top of oceanic basement is clearly imaged in the trench on all the seismic profiles, and a clear basement reflection can be traced continuously deeper into the subduction zone to at least 60–70 km from the deformation front, the location of the forearc high (Fig. 2; Fig. DR1). In several places, reflections from prism faults merge at depth with the oceanic basement reflection (Cook et al., 2014). From this relationship and the downdip continuity, we interpret that the décollement is at the top of basement. We collected an approximate strike profile (Figs. 1 and 2; Fig. DR1), positioned so that oceanic basement was clearly imaged and not obscured by multiples; the oceanic basement reflection is also largely continuous on this profile.

The shallow downgoing oceanic plate generally dips 7°–9° (e.g., Fig. 2 profiles SUMD14 and SUMD07), except for a restricted zone west of the Batu Islands; profile SUMD09 shows a lower dip of 5°–6° on the top of the oceanic basement. Consequently, at the landward end of SUMD09 the plate is 3 km shallower than at equivalent positions along adjacent profiles (Fig. 2). The same topographic feature is seen on strike line SUMD30, which shows an oceanic crustal reflection 3 km shallower between 95 km and 110 km on the profile. Shallow seismic velocity variations through the thin sediments and bathymetric effects (removed by the depth conversion) cannot explain this difference. Explaining the shallow basement with a localized seismic velocity anomaly would require a 20% increase in velocity from the seabed through the prism; this is unlikely because there are no similar features elsewhere within the MCS data. In addition, fracturing and increased fluid content that might be expected around subducting topography (von Huene et al., 2004; Mochizuki et al., 2008) would reduce, not increase, seismic velocity. Thus, we conclude that the observed high is true basement relief.

BASEMENT TOPOGRAPHY FROM GRAVITY DATA

We analyzed the free air gravity anomaly (FAA; Fig. DR3) using both shipboard and satellite-derived data. We removed the attraction of the seabed by applying the method of Parker (1973) to the bathymetry grid, with a seabed density contrast of 850 kg/m^3 from comparison of gravity and bathymetry data (see the Data Repository) to produce a residual gravity anomaly (Fig. 3). This residual anomaly represents the effect of deeper density contrasts, with negative values indicating low densities and positive values indicating high densities.

The trend in residual gravity from positive anomalies outboard of the trench to negative beneath the forearc basin represents deepening of the slab. Beneath the accretionary prism a more complex pattern of positive and negative residuals shows lateral density changes. Three regions of positive residual gravity are present beneath the accretionary prism: (1) offshore Nias, positive residuals correspond to an area of active uplift (Cook et al., 2014); (2) offshore the Batu Islands, a series of positive residuals are immediately adjacent to the location of the extinct WFR (Liu et al., 1983); and (3) offshore Siberut, positive residuals align with fracture zones in the subducting plate.

ORIGIN AND EFFECTS OF BASEMENT TOPOGRAPHY

Two of the residual gravity highs beneath the prism do not correspond to such clear oceanic basement relief in the MCS data: offshore Nias (1, Fig. 3), the region of active uplift may instead be associated with higher densities within the prism due to erosion and reaccretion of older compacted forearc material. Offshore Siberut the north-south–trending positive residual gravity region (3, Fig. 3) is along strike from features in the IFZ; however, this terminates in a gravity low offshore the Batu Islands.

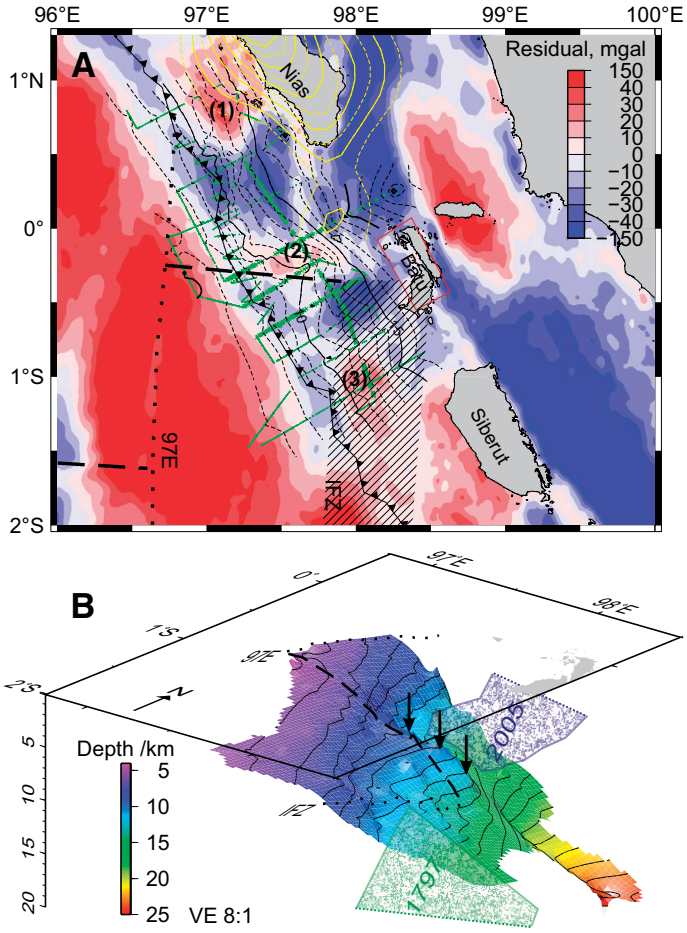

Figure 3. A: Residual gravity anomaly after removing the signature of bathymetry from satellite gravity (Sandwell et al., 2013) using effective density contrast of 850 kg/m^3; red shows mass excess and blue shows mass deficit. Black contours show depth to top of subducting plate from multichannel seismic reflection data; dashed lines are 1 km intervals and heavy lines are 5 km intervals; green dots show picks. Yellow contours show A.D. 2005 coseismic slip (Hsu et al., 2006); red box indicates the 1935 earthquake fault plane (Natawidjaja et al., 2004). 1–3—residual gravity highs (see text); 97E, IFZ—97E and Investigator fracture zones. B: Three-dimensional perspective view of the top of oceanic basement with 2005 coseismic slip (Hsu et al., 2006) and the estimated 1797 rupture (Natawidjaja et al., 2006); note that both rupture regions continue outside this figure. The basement high that stopped the 2005 rupture is shown by the arrows. VE—vertical exaggeration.

Although elevated basement is present outboard of the trench along the northern part of the IFZ, the MCS (see Fig. DR7) and gravity data beneath the prism suggest that any equivalent basement relief varies rapidly along strike, likely due to plate reorganization during the last stages of WFR spreading. The detailed rupture of the A.D. 1797 earthquake is not sufficiently well constrained to assess any role these features may have.

The third positive residual gravity region (2, Fig. 3) offshore the Batu Islands matches the 15 km × 30 km region where the MCS data suggest a 3 km shallowing of the downgoing plate. The local structural framework supports shallow oceanic basement here: the inside corner between a slow-spreading ridge axis and a transform fault is often a topographic high (Severinghaus and Macdonald, 1988). Immediately west of the trench, where the relict WFR intersects the 97EFZ, basement shallows by ~3 km, forming a bathymetric high on the southern (inside) corner. The basement anomaly beneath the subduction zone is an equivalent inside corner between the WFR and the northernmost part of the IFZ (Fig. 3).

[1]GSA Data Repository item 2016017, additional details of the gravity methods and a discussion of the location of the IFZ, is available online at www.geosociety.org/pubs/ft2016.htm, or on request from editing@geosociety.org or Documents Secretary, GSA, P.O. Box 9140, Boulder, CO 80301, USA.

The 3 km elevation difference is above the threshold identified by Sparkes et al. (2010) as the minimum to affect earthquake segmentation. Global positioning system data from the islands (Hsu et al., 2006) show that southward propagation of the A.D. 2005 rupture ceased at the subducted basement high (Fig. 3). This also corresponds with a southeastward onset of recent reduced plate coupling (Chlieh et al., 2008). We therefore suggest that the basement high causes a fundamental segment boundary within the subduction zone. The lack of earthquake epicenters in both local and long-term teleseismic data sets (Fig. 1) suggests that the basement high is genuinely aseismic over the data set period; this is more consistent with a locally locked plate boundary than continuous creep, which would be expected to generate small but locally detectable earthquakes. We suggest therefore that subducting topography produces a locally strong plate boundary that stops large earthquake rupture (such as in 2005), for example by increasing friction or by bridging the décollement. This dominates any weakening of the plate boundary that may result from extra fluids or faulting around the basement high. While the two most recent major events have been stopped by this barrier, infrequent rupture generating very large earthquakes cannot be ruled out, and the paleoseismic record should be examined for this possibility.

ACKNOWLEDGMENTS

This work was funded by Natural Environment Research Council grant NE/D004231/1. Cook was funded by the Natural Sciences and Engineering Research Council of Canada and the University of Southampton. We thank the officers, crew, and other participants on F/S *Sonne* cruises SO198–2 and SO200, as well as our partners in Badan Pengkajian dan Penerapan Teknologi (BPPT), Jakarta, for their logistical support. We also thank reviewers A. Meltzner, N. Hovius, and J. Dyment for their comments, which significantly improved the manuscript.

REFERENCES CITED

Bilek, S.L., Schwartz, S.Y., and DeShon, H.R., 2003, Control of seafloor roughness on earthquake rupture behavior: Geology, v. 31, p. 455–458, doi:10.1130/0091-7613(2003)031<0455:COSROE>2.0.CO;2.

Chlieh, M., Avouac, J.P., Sieh, K., Natawidjaja, D.H., and Galetzka, J., 2008, Heterogeneous coupling of the Sumatran megathrust constrained by geodetic and paleogeodetic measurements: Journal of Geophysical Research, v. 113, B05305, doi:10.1029/2007JB004981.

Cloos, M., 1992, Thrust-type subduction-zone earthquakes and seamount asperities: A physical model for seismic rupture: Geology, v. 20, p. 601–604, doi:10.1130/0091-7613(1992)020<0601:TTSZEA>2.3.CO;2.

Cook, B.J., Henstock, T.J., McNeill, L.C., and Bull, J.M., 2014, Controls on spatial and temporal evolution of prism faulting and relationships to plate boundary slip offshore north-central Sumatra: Journal of Geophysical Research, v. 119, p. 5594–5612, doi:10.1002/2013JB010834.

Hsu, Y.-J., Simons, M., Avouac, J.-P., Galetzka, J., Sieh, K., Chlieh, M., Natawidjaja, D., Prawirodirdjo, L., and Bock, Y., 2006, Frictional afterslip following the 2005 Nias-Simeulue earthquake, Sumatra: Science, v. 312, p. 1921–1926, doi:10.1126/science.1126960.

Jacob, J., Dyment, J., and Yatheesh, V., 2014, Revisiting the structure, age, and evolution of the Wharton Basin to better understand subduction under Indonesia: Journal of Geophysical Research, v. 119, p. 169–190, doi:10.1002/2013JB010285.

Kelleher, J., and McCann, W., 1976, Buoyant zones, great earthquakes, and unstable boundaries of subduction: Journal of Geophysical Research, v. 81, p. 4885–4896, doi:10.1029/JB081i026p04885.

Kieckhefer, R.M., Shor, J.G., Jr., and Curray, J.R., 1980, Seismic refraction studies of the Sunda trench and forearc basin: Journal of Geophysical Research, v. 85, p. 863–889, doi:10.1029/JB085iB02p00863.

Kopp, H., 2013, The control of subduction zone structural complexity and geometry on margin segmentation and seismicity: Tectonophysics, v. 589, p. 1–16, doi:10.1016/j.tecto.2012.12.037.

Kopp, H., et al., 2008, Lower slope morphology of the Sumatra trench system: Basin Research, v. 20, p. 519–529, doi:10.1111/j.1365-2117.2008.00381.x.

Lange, D., Tilmann, F., Rietbrock, A., Collings, R., Natawidjaja, D.H., Sawargadi, B.W., Barton, P., Henstock, T., and Ryberg, T., 2010, The fine structure of the subducted Investigator Fracture Zone in Western Sumatra as seen by local seismicity: Earth and Planetary Science Letters, v. 298, p. 47–56, doi:10.1016/j.epsl.2010.07.020.

Liu, C., Curray, J.R., and McDonald, J.M., 1983, New constraints on the tectonic evolution of the eastern Indian Ocean: Earth and Planetary Science Letters, v. 65, p. 331–342, doi:10.1016/0012-821X(83)90171-1.

McNeill, L.C., and Henstock, T.J., 2014, Forearc structure and morphology along the Sumatra-Andaman subduction zone: Tectonics, v. 33, p. 112–134, doi:10.1002/2012TC003264.

Meltzner, A.J., et al., 2015, Time-varying interseismic strain rates and similar seismic ruptures on the Nias-Simeulue patch of the Sunda megathrust: Quaternary Science Reviews, v. 122, p. 258–281, doi:10.1016/j.quascirev.2015.06.003.

Mochizuki, K., Yamada, T., Shinohara, M., Yamanaka, Y., and Kanazawa, T., 2008, Weak interplate coupling by seamounts and repeating M ~7 earthquakes: Science, v. 321, p. 1194–1197, doi:10.1126/science.1160250.

Natawidjaja, D.H., Sieh, K., Ward, S.N., Cheng, H., Edwards, R.L., Galetzka, J., and Suwargadi, B.W., 2004, Paleogeodetic records of seismic and aseismic subduction from central Sumatran microatolls, Indonesia: Journal of Geophysical Research, v. 109, B04306, doi:10.1029/2003JB002398.

Natawidjaja, D.H., Sieh, K., Chlieh, M., Galetzka, J., Suwargadi, B.W., Cheng, H., Edwards, R.L., Avouac, J.-P., and Ward, S.N., 2006, Source parameters of the great Sumatran megathrust earthquakes of 1797 and 1833 inferred from coral microatolls: Journal of Geophysical Research, v. 111, B06403, doi:10.1029/2005JB004025.

Newcomb, K., and McCann, W., 1987, Seismic history and seismotectonics of the Sunda Arc: Journal of Geophysical Research, v. 92, p. 421–439, doi:10.1029/JB092iB01p00421.

Parker, R.L., 1973, The rapid calculation of potential anomalies: Royal Astronomical Society Geophysical Journal, v. 31, p. 447–455, doi:10.1111/j.1365-246X.1973.tb06513.x.

Prawirodirdjo, L., McCaffrey, R., Chadwell, C.D., Bock, Y., and Subarya, C., 2010, Geodetic observations of an earthquake cycle at the Sumatra subduction zone: Role of interseismic strain segmentation: Journal of Geophysical Research, v. 115, B03414, doi:10.1029/2008JB006139.

Royer, J.-Y., and Sandwell, D.T., 1989, Evolution of the eastern Indian Ocean since the Late Cretaceous: Constraints from Geosat altimetry: Journal of Geophysical Research, v. 94, p. 13,755–13,782, doi:10.1029/JB094iB10p13755.

Sandwell, D.T., Garcia, E., Soofi, K., Wessel, P., Chandler, M., and Smith, W.H.F., 2013, Towards 1 mGal global marine gravity from CryoSat-2, Envisat, and Jason-1: The Leading Edge, v. 32, p. 892–899, doi:10.1190/tle32080892.1.

Scholz, C.H., and Small, C., 1997, The effect of seamount subduction on seismic coupling: Geology, v. 25, p. 487–490, doi:10.1130/0091-7613(1997)025<0487:TEOSSO>2.3.CO;2.

Severinghaus, J.P., and Macdonald, K.C., 1988, High inside corners at ridge-transform intersections: Marine Geophysical Researches, v. 9, p. 353–367, doi:10.1007/BF00315005.

Shulgin, A., Kopp, H., Klaeschen, D., Papenberg, C., Tilmann, F., Flueh, E.R., Franke, D., Barckhausen, U., Krabbenhoeft, A., and Djajadihardja, Y., 2013, Subduction system variability across the segment boundary of the 2004/2005 Sumatra megathrust earthquakes: Earth and Planetary Science Letters, v. 365, p. 108–119, doi:10.1016/j.epsl.2012.12.032.

Singh, S.C., et al., 2011, Aseismic zone and earthquake segmentation associated with a deep subducted seamount in Sumatra: Nature Geoscience, v. 4, p. 308–311, doi:10.1038/ngeo1119.

Sparkes, R., Tilmann, F., Hovius, N., and Hillier, J., 2010, Subducted seafloor relief stops rupture in South American great earthquakes: Implications for rupture behaviour in the 2010 Maule, Chile earthquake: Earth and Planetary Science Letters, v. 298, p. 89–94, doi:10.1016/j.epsl.2010.07.029.

Tilmann, F.J., Craig, T.J., Grevemeyer, I., Suwargadi, B., Kopp, H., and Flueh, E., 2010, The updip seismic/aseismic transition of the Sumatra megathrust illuminated by aftershocks of the 2004 Aceh-Andaman and 2005 Nias events: Geophysical Journal International, v. 181, p. 1261–1274, doi:10.1111/j.1365-246X.2010.04597.x.

von Huene, R., Ranero, C.R., and Vannucchi, P., 2004, Generic model of subduction erosion: Geology, v. 32, p. 913–916, doi:10.1130/G20563.1.

Wang, K., and Bilek, S.L., 2011, Do subducting seamounts generate or stop large earthquakes?: Geology, v. 39, p. 819–822, doi:10.1130/G31856.1.

Manuscript received 12 August 2015
Revised manuscript received 13 November 2015
Manuscript accepted 23 November 2015

Printed in USA